NANO LETTERS

Letter

pubs.acs.org/NanoLett

Kondo Effect in a Neutral and Stable All Organic Radical Single Molecule Break Junction

Riccardo Frisenda,[†] Rocco Gaudenzi,[†] Carlos Franco,[‡] Marta Mas-Torrent,[‡] Concepció Rovira,[‡] Jaume Veciana,[‡] Isaac Alcon,[§] Stefan T. Bromley,[§,∥] Enrique Burzurí,*[,†] and Herre S. J. van der Zant[†]

[†]Kavli Institute of Nanoscience, Delft University of Technology, Lorentzweg 1, 2628 CJ, Delft, The Netherlands

[‡]Institut de Ciéncia de Materials de Barcelona (ICMAB-CSIC) and CIBER-BBN, Campus de la UAB, 08193, Bellaterra, Spain

[§]Departament de Química Física and Institut de Química Teórica i Computacional (IQTCUB), Universitat de Barcelona, E-08028 Barcelona, Spain

[∥]Institició Catalana de Recerca i Estudis Avançats (ICREA), 08010 Barcelona, Spain

S *Supporting Information*

ABSTRACT: Organic radicals are neutral, purely organic molecules exhibiting an intrinsic magnetic moment due to the presence of an unpaired electron in the molecule in its ground state. This property, added to the low spin−orbit coupling and weak hyperfine interactions, make neutral organic radicals good candidates for molecular spintronics insofar as the radical character is stable in solid state electronic devices. Here we show that the paramagnetism of the polychlorotriphenylmethyl radical molecule in the form of a Kondo anomaly is preserved in two- and three-terminal solid-state devices, regardless of mechanical and electrostatic changes. Indeed, our results demonstrate that the Kondo anomaly is robust under electrodes displacement and changes of the electrostatic environment, pointing to a localized orbital in the radical as the source of magnetism. Strong support to this picture is provided by density functional calculations and measurements of the corresponding nonradical species. These results pave the way toward the use of all-organic neutral radical molecules in spintronics devices and open the door to further investigations into Kondo physics.

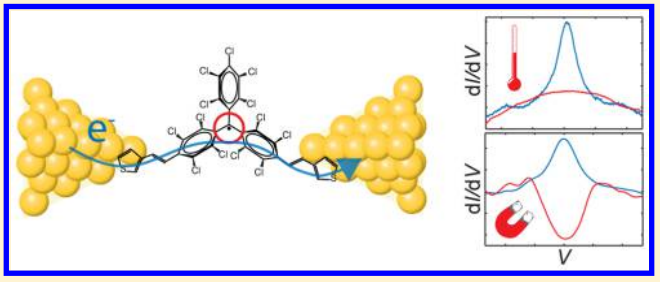

KEYWORDS: *Single molecule, break junction, electrical transport, Kondo effect, organic radical, magnetism*

Organic free radicals were first synthesized in the 1900s and recently have been explored as building blocks for magnetic materials.[1−3] Thanks to the unpaired electron, these molecules are paramagnetic in their neutral state and have low spin−orbit coupling and weak hyperfine interactions due to their all-organic composition. Because of these properties, absent in transition metal-based magnetic compounds, organic radicals have recently attracted attention in molecular spintronics,[4,5] where long spin coherence times are required to preserve the information encoded in the electronic spin.

A number of studies on transport through organic radicals have lately appeared both on assemblies as well as individual molecules. An example of the first type can be found in refs 6−8, where a self-assembled monolayer of radical molecules is studied employing a conductive AFM. Investigations on individual molecules have been only focused on scanning tunneling spectroscopy studies of the Kondo effect in π-extended organic radical molecules physisorbed on surfaces.[9−11] However, a demonstration that a neutral organic radical molecule can retain its magnetic moment when integrated in a solid-state device, a crucial step toward future spintronics applications, is so far absent, which is in contrast to analogous results reported for molecules containing transition metals.[12]

In this Letter, we report on the detection of the unpaired spin of a neutral and stable polychlorotriphenylmethyl (PTM) radical molecule combining for the first time two and three-terminal solid-state devices. The detection is based on the observation of a Kondo resonance, arising from the many-body interaction between the conduction electrons and the magnetic impurity.[13,14] Kondo temperatures T_K of about 3 K are extracted and found to be rather independent of the elastic/inelastic conductance background and mechanical displacement of the junction, which is in contrast with other molecular families.[12,15] In addition, measurements on the nonradical PTM-αH counterpart show no Kondo signatures. These observations strongly support the picture that the magnetic impurity originates from the radical unpaired electron: a magnetic impurity well-protected against variations of the molecular arrangement and weakly coupled to the electron bath in the leads. This intrinsic Kondo effect in a neutral molecule

Received: January 14, 2015
Revised: March 17, 2015

DOI: 10.1021/acs.nanolett.5b00155
Nano Lett. XXXX, XXX, XXX−XXX

should be contrasted to the one observed in other organic molecules[15−19] where the magnetism is induced by a delocalized charge added with a gate voltage or by electron transfer from the leads, that is, in molecular systems that are charged and not intrinsically paramagnetic in their neutral state. This Kondo effect should also be contrasted with the one observed in transition metal-based molecules.[12,20,21] Kondo physics in these molecules arises from 3d orbitals making the Kondo temperature sensitive to external stimuli like stretching[12] or voltage.[21] Moreover, for spintronics purposes 3d orbitals of transition metals are expected to contribute more to the spin decoherence of the flowing electrons compared to the p orbitals of organic radicals.

A schematic of the PTM radical molecule is presented in Figure 1a. The unpaired electron is mainly located in the

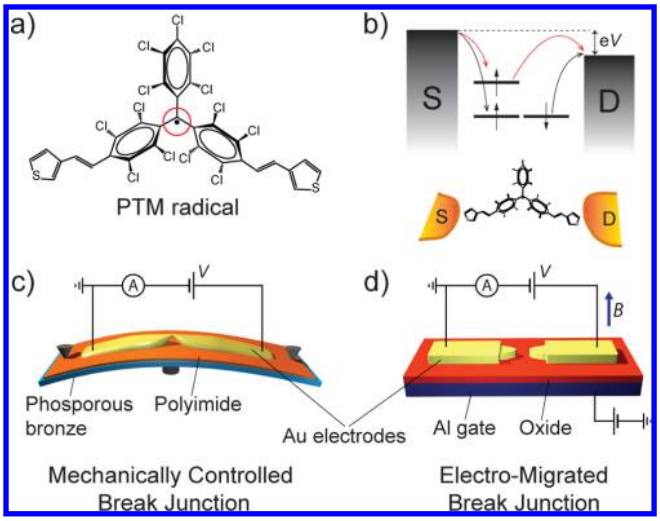

Figure 1. Two and three-terminal PTM radical-based devices. (a) Sketch of the neutral PTM radical molecule. The radical center resides on the carbon atom located in the middle of three chlorinated phenyl rings and is marked with a red circle. (b) Simple model of the energy levels/orbitals involved in the transport through the molecule. The HOMO orbital accounts for the spin-unpolarized background transport (black arrows), the radical-deriving SOMO orbital is the source of spin-correlated transport (red arrows). Below, the ideal arrangement of the molecule between source (S) and drain (D) electrodes is shown. (c) Two-terminal mechanically controlled break junction device. (d) Three-terminal electromigrated break junction transistor.

trivalent central carbon atom, shielded by three chlorinated phenyl rings arranged in a propeller-like configuration that provide stability against chemical reactions (see ref 22 and references therein). Two additional thiophene rings are bonded, through ethylene bridges, to the triphenylmethyl backbone and serve as linkers to the gold electrodes (Au−S interactions). The ideal physical arrangement of the molecule between the source and drain electrodes and the associated off-resonant transport schematic are depicted in Figure 1b. We can identify a spin-unpolarized background transport channel (black arrows) through the highest occupied molecular orbital (HOMO) and a spin-flipping Kondo-mediated transport channel (red arrows). This additional channel arises from the singly occupied molecular orbital (SOMO) and is responsible for the paramagnetism.

Measurements on the molecule were performed in two complementary setups: the two-terminal mechanically controlled break junction (MCBJ) and the three-terminal electromigrated break junction (EMBJ) setups, respectively depicted schematically in Figure 1c,d. MCBJs allowed for a study of the Kondo feature on a large number of samples as a function of electrode displacement. More extended detailed measurements as a function of temperature, magnetic field, and gate voltage were conducted with the EMBJs.

Results. *Mechanically Controlled Break Junctions.* Low-temperature $I-V$ measurements are carried out on PTM molecular junctions formed with MCBJ nanoelectrodes. Here a large number of single-molecule junctions and different molecule−metal configurations can be studied by repeatedly breaking up the electrodes and pushing them together. We have measured in total 86 junctions in the presence of the PTM radical from which 31 formed molecular junctions. Interestingly, 20% of the molecular junctions showed a zero-bias peak in the differential conductance dI/dV. Figure 2a shows the

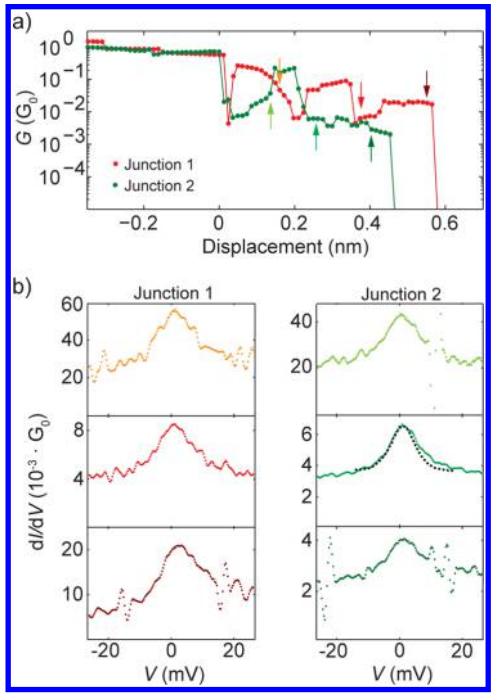

Figure 2. Two PTM radical samples showing a Kondo resonance investigated with mechanically controlled break junctions. (a) Conductance versus displacement traces for two different junctions measured with MCBJ. Each data point is extracted from an individual $I-V$. (b) Differential conductance traces measured at displacements indicated by the arrows in (a). Measurements are taken at $T \approx 6$ K. The dashed line corresponds to a different measurement on a PTM radical in EMBJ at $T \approx 4.5$ K. The trace is offset vertically. The FWHM and the conductance levels are comparable with both techniques. The slight variations in the peak width and the noise level may be due to coupling fluctuations at the molecule/metal interface while stretching.

zero-bias conductance, extracted from $I-V$s at the corresponding position, as a function of the electrode displacement for two different PTM radical junctions. Both conductance traces show a plateau at 1 G_0 due to transport through a single Au atom, indicating atomically sharp electrodes. For conductance values below 1 G_0, the molecular junctions exhibit plateaus; this nonexponential decay with the interelectrode distance signals the presence of a molecule. At displacements of about 0.5 nm, both junctions exhibit an abrupt jump to conductance values

DOI: 10.1021/acs.nanolett.5b00155
Nano Lett. XXXX, XXX, XXX−XXX

below the noise level of 10^{-6} G_0, indicating the rupture of the molecular junction. The fluctuations observed in conductance around the 10^{-2} G_0 value are to be assigned to atomic rearrangements at the metal/molecule interface or inside the molecule.[23,24] The current I is measured versus bias voltage V at every step of the junction stretching and thereafter dI/dV is obtained by taking the numerical derivative with respect to V. Figure 2b shows three examples at the positions marked by the colored arrows in Figure 2a. All traces show a zero-bias anomaly that persists along the stretching of the junction even if the average conductance background changes. Such mechanical stability indicates that the origin of the zero-bias anomaly is intrinsic to the PTM radical molecule and is not sensitive to stretching-dependent variations of the interface between the anchoring groups and the electrodes, in contrast to refs 12 and 15.

As a reference, we have also measured 95 junctions in the presence of the nonradical αH counterpart. Molecular junctions are formed in 30 cases, making the junction formation probability approximately the same for the radical and nonradical species and equal to 35%. In contrast to the radical molecule, the nonradical one shows no zero-bias peak in all the cases, see Supporting Information. In this way we can ascribe the origin of the zero-bias resonance to an intrinsic property of the radical molecule, as compared to the nonradical one. Provided that the only difference between radical and nonradical molecule lies in the open or closed shell electronic structure, it is reasonable to assign the zero-bias feature to the presence of the unpaired electron in the radical. In order to verify the Kondo character of this zero-bias resonance, measurements in temperature and magnetic field are carried out.

Electromigrated Break Junctions. To investigate in more detail the zero-bias resonance we have employed the EMBJ setup. With this setup, we perform low-noise measurements at temperatures ranging from $T \approx 30$ mK to $T \approx 4.5$ K, magnetic fields up to 8 T, and gate voltage. Nanojunctions are prepared following the electromigration method.[25,26] This technique, together with device fabrication, preparation, and deposition of the molecular solution, is described in Methods section. We record the formation of 25 molecular junctions out of the 126 measured devices. From those, a zero-bias peak in dI/dV appears in 11 samples. Differential conductance measurements as a function of the gate voltage showed off-resonant transport in the entire accessible gate window, see Supporting Information. This is a fingerprint of a substantial HOMO–LUMO gap. In Figure 3, the temperature and magnetic field characterization for two samples are presented. Figure 3a,b shows dI/dV spectra at different temperatures. A zero-bias resonance is clearly visible. In Figure 3c,d, the corresponding conductance at $V = 0$, $dI/dV|_{V=0}$, is plotted as a function of temperature on a logarithmic scale. The typical temperature dependence expected from a Kondo resonance is observed, ranging from the intermediate (weak coupling) $T \approx T_K$ to the low-energy (strong coupling) regime for $T \ll T_K$, where the asymptotic value of $dI/dV|_{V=0}$ is reached. For a direct comparison between traces shown here in the weak coupling regime and those measured with the MCBJ in Figure 2, we refer the reader to the Supporting Information. We notice here the three-order of magnitude difference in the conductance values observed between sample A and sample B. In addition, in Figure 3b two side shoulders weakly dependent on temperature are visible; such steplike features, occurring also

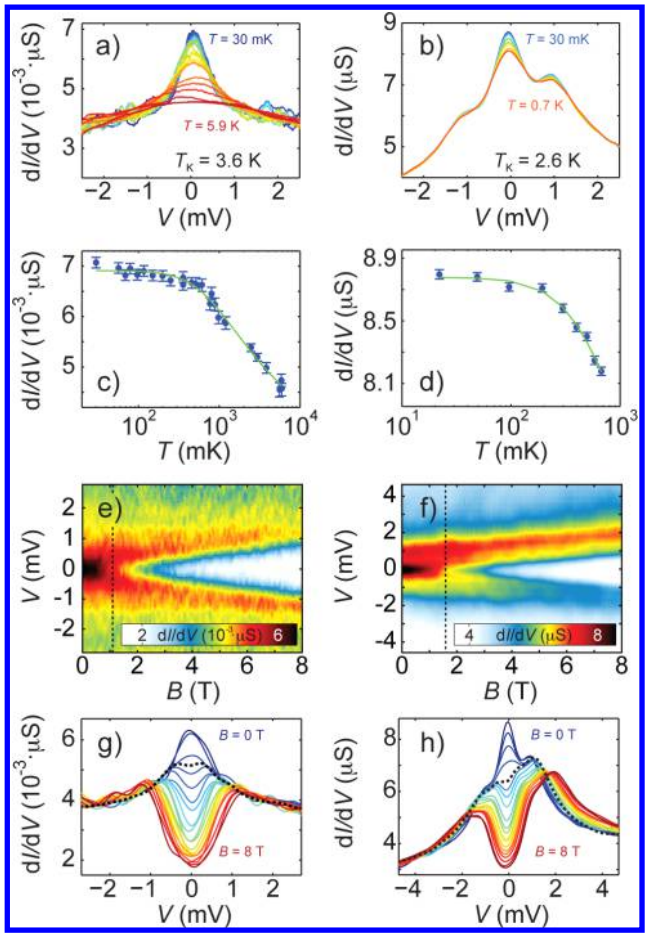

Figure 3. Two PTM radical samples exhibiting Kondo resonance investigated with electromigrated break junctions. (a,b) dI/dV traces ($1G_0 \approx 77$ μS) of the radical for temperatures indicated in the panels. (c,d) Peak height ($dI/dV|_{V=0}$), extracted from (a,b), as a function of temperature on a logarithmic scale. The solid lines are fits to a spin-1/2 Kondo with parameters $G_0 = 3.8$ nS, $G_b = 3.1$ nS, and $T_K = 3.6$ K for (c) and $G_0 = 3.1$ nS, $G_b = 5.6$ nS, and $T_K = 2.6$ K for (d) (see text). (e,f) dI/dV color map measured as a function of the magnetic field B and bias voltage V at $T = 590$ mK and $T = 25$ mK, respectively. Black dashed lines mark the onset of Kondo splitting. (g,h) dI/dV spectra extracted from (e,f) with a regular spacing of $\Delta B = 0.4$ T. The Kondo peak is seen splitting at $B_c \approx 1.2$ T and $B_c \approx 1.6$ T, respectively, as black dashed traces indicate.

at higher harmonically spaced bias values, are observed in about 50% of the measured samples. The harmonic spacing together with their nonexponential temperature dependence indicate a vibrational origin.[27,28]

A fit to the formula describing the conductance G as a function of the temperature for spin-1/2 Kondo[29]

$$G(T) = G_0\left[1 + (2^{1/0.21} - 1)\left(\frac{T}{T_K}\right)^2\right]^{-0.21} + G_b \quad (1)$$

yields $T_K = 3.6$ K and $T_K = 2.6$ K for the first and second samples, respectively. In 1, G_0 is the conductance in the $T \to 0$ limit, G_b is the background contribution, and T_K is defined so that $G(T_K) - G_b = G_0/2$. From the lower temperature spectra ($T \ll T_K$) of Figure 3a,b, that is, the data points in the flat region of Figure 3c,d, an independent estimation of the Kondo temperature can be obtained. Fitting the Kondo peak with a Lorentzian, the Kondo temperature is extracted from the full

DOI: 10.1021/acs.nanolett.5b00155
Nano Lett. XXXX, XXX, XXX–XXX

width at half-maximum (Γ_K) of the Lorentzian according to $\Gamma_K \approx 2\sqrt{2}k_B T_K$.[30] The obtained values 3.0 and 3.1 K are in agreement with those deduced from the fit to 1.

In Figure 3e,f, the magnetic field dependence of dI/dV in the strong coupling regime ($T \ll T_K$) is shown. Suppression and subsequent Zeeman splitting of the Kondo resonance are observed. An estimation of the g-factor from the Zeeman energy in magnetic field yields $g \approx 2.0 \pm 0.2$. Figure 3g,h displays regularly spaced ($\Delta B = 0.4$ T) linecuts extracted from Figure 3e,f. At $B_c \approx 1.2$ T and $B_c \approx 1.6$ T, respectively, the onset of the Kondo resonance splitting is visible, as marked by the dashed lines in Figure 3e,f. These values are consistent with the expected critical magnetic field given by $B_c \approx 0.5k_B T_K/(g\mu_B)$,[31] above which splitting of the Kondo peak should be observed. Particularly insightful is the field-dependence in Figure 3h, where the Kondo resonance is observed evolving on top of the two side shoulders in an independent way. This behavior further supports the idea of a distinct origin for the two features.

The measurements in the EMBJ setup show a Kondo state in the strong coupling regime in which the three different perturbations all show the expected behavior.[10] This provides a sound estimation of the Kondo temperatures involved. Interestingly, the conductance levels $dI/dV|_{V=0}$ of the two samples shown in Figure 3 exhibit a three-order of magnitude difference due to an increase of the background conductance G_b with a similar G_0/G_b ratio in both cases.

Discussion. To corroborate the experimental findings, we carried out density functional theory (DFT) calculations to model the ground state electronic properties of the PTM radical. We employed the B3LYP hybrid functional[32] with a triple-ζ basis set incorporating polarization and diffuse functions for all atoms. Orbital energies were obtained after first optimizing the structure of the radical molecule in free space using spin-unrestricted calculations with no symmetry constrains. The Gaussian 09 code[33] was used throughout. Optimization of the molecule together with Au atoms to mimic the presence of the electrodes does not show significant variations in the geometric or electronic structure (see Methods). Figure 4 shows the calculated energy level diagram of the valence orbitals of the PTM radical molecule for the two spin channels α and β. HOMO and LUMO exhibit spin degeneracy, while SOMO and LUMO-β are spin-polarized. The experimental Fermi energy of gold lies close to the middle of the SOMO−LUMO-β energy gap (2 eV). The radical unpaired electron in the SOMO is therefore responsible for the magnetic properties of the system. The proximity of the Fermi level to the HOMO and SOMO occupied levels makes them the most relevant for transport, yielding an hole-mediated off-resonant conductance pathway. The large gap and the position of the Fermi energy are in agreement with the off-resonant transport experimentally observed in the whole gate voltage range, see Supporting Information. The large gap is also consistent with the stability of the Kondo resonance under external variations of the electrostatic environment.

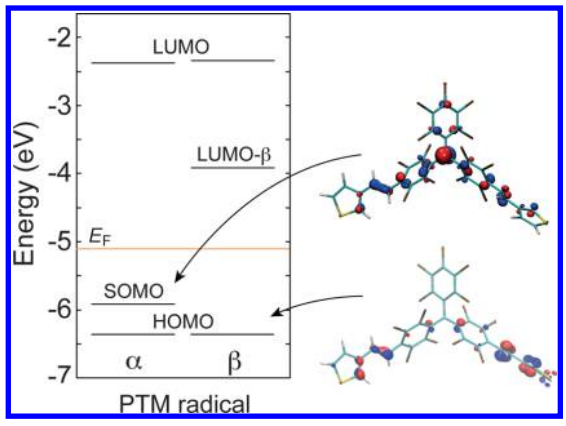

Figure 4. Density functional theory calculations. DFT energy level diagram for the two spin channels α and β of the PTM-radical molecule. The orange line indicates the theoretical Fermi energy of gold. HOMO and SOMO levels are depicted together with their relative isosurfaces.

A comparison between the iso-surfaces of the SOMO and the HOMO shows the former as mostly localized on the radical carbon atom with a small component on the backbone and the latter as fully delocalized over the molecular backbone with a considerable weight on the thiophene groups. Worth noticing is the two-lobed p-like shape of the SOMO, indicating a weak hybridization of the atomic orbital and its strong atomic character. Within this framework, we can propose a coherent picture to account for the transport through the PTM radical molecule observed in the experiments. The HOMO provides the spin-independent conductance background, while the SOMO is responsible for the Kondo-correlated phenomena. The strong localization of the SOMO in the carbon protected by the three chlorinated phenyl rings makes the Kondo resonance stable and reproducible in different samples and under stretching. To complete the analysis, DFT calculations using the same model were conducted for the PTM-αH nonradical molecule and the stretched PTM-radical molecule. The energy diagram and isosurfaces of the relevant orbitals are reported in the Supporting Information. The calculations for the PTM-αH nonradical reveal the presence of a fully occupied HOMO with the absence of a SOMO level and its unpaired electron spin. These findings are again in accordance with the experimental absence of Kondo features in the PTM-αH-formed junctions. For the stretched PTM-radical molecule, the energy of the SOMO varies only slightly throughout the stretching. This is in line with the localized character of the SOMO and the experimental findings (see Supporting Information).

Conclusion. Summarizing, we contacted a neutral organic radical molecule in both two and three-terminal solid-state devices. We demonstrate that the magnetic moment of the PTM-radical open-shell system is preserved upon interaction with the metal electrodes and robust against mechanical/electrostatical changes at the electrode-molecule interface. We do this by measuring in mechanically controlled break junctions as well as electro-migrated break junctions a statistically significant presence of fully screened spin-1/2 Kondo features that are insensitive to the electrode displacement and background conductance. We attribute the source of the paramagnetism to the unpaired electron located in the radical carbon center and we substantiate the picture with DFT calculations. Measurements on the closed-shell αH nonradical molecule show no Kondo correlations and therefore corroborate the relation between radical center and magnetic properties. The findings reported here open up the way toward the use of all-organic radical molecules in spintronics devices. From a more fundamental point of view, the overall stability of the unpaired electron of the radical molecule makes it an excellent platform for further investigation on Kondo physics.

DOI: 10.1021/acs.nanolett.5b00155
Nano Lett. XXXX, XXX, XXX−XXX

Methods. *Synthesis of PTM Radical and PTM-αH.* The PTM-αH molecule has been synthesized using a Wittig-type coupling between polychlorinated triphenylmethane bisphosphonate and the 1-thiophenecarboxaldehyde. Treatment of PTM-αH with tetrabutylammonium hydroxide promotes the removal of the acidic proton at the αH position to give the corresponding carbanion that was subsequently oxidized with p-chloranil giving the desired PTM radical.

Preparation of the Solution. The molecular solutions are prepared in a glove-box dissolving 1.8 mg of PTM radical or PTM-αH in 2 mL of nitrogen saturated dichlorobenzene [c = 1 mM].

Mechanically Controlled Break Junctions (MCBJ). The mechanically controlled break junctions experiment is performed in vacuum ($p = 1.0 \times 10^{-7}$ mbar) at liquid He temperature. The molecular solution is drop-casted onto the MBCJ sample, whose fabrication is describe elsewhere,[34,35] and the setup is evacuated and cooled down to liquid He temperature. Measurements begin with a metallic constriction, characterized by a conductance of 10 G_0 that, by bending the substrate, can be stretched until it breaks in two nanoelectrodes facing each other, which can eventually be bridged by a molecule. The nanoelectrodes position can be controlled, and by uniting them one can form a new metallic constriction, allowing the exploration of many different junction configurations. During the stretching of the wire, performed in steps of 10 pm, we measure $I-V$ characteristics for each position and control the bending with a feedback on the current/conductance.

Electro-Migrated Break Junctions (EMBJ). Measurements in the electromigrated break junctions are carried out in vacuum ($p < 1.0 \times 10^{-3}$ mbar) in a dilution fridge with a base temperature of 30 mK. Magnetic fields up to 8 T can be applied to the sample. The molecular solution is drop-casted onto a Si/SiO_2 chip containing an array of 24 Au bridges 100 nm wide, 400 nm long, and 12 nm thick with an Al/Al_2O_3 local gate underneath. A nanogap is produced by feedback-controlled electromigration[25] of each of these bridges. As the bridge conductance reaches 3−4 G_0, electromigration is stopped and the wire is let self-break at room temperature.[26] The molecular solution is evaporated while evacuating the chamber and the sample is cooled down. All measurements are performed in dc with low-noise homemade electronics.

DFT Calculations. The molecular geometries of both the radical (spin unrestricted) and the H (closed shell) were optimized with no symmetry constraints using density functional theory as implemented in the Gaussian 09 code.[33] In all cases, the B3LYP[32] hybrid exchange-correlation functional and a triple-ζ 6-311++G(d,p) basis set including polarization functions on all atoms was employed. Different configurations of the PTM molecule, corresponding to different possible orientations of the C═C-linked thyophene rings were tested in both its radical and αH forms. The lowest energy configurations were then used to extract the reported orbital energies. Optimizations of the PTM molecules with Au atoms placed near the two sulfur atoms to mimic the presence of gold contacts were found to very slightly stabilize all orbital energies by 0.05−0.1 eV. The significant dispersive contribution to the Au−S interaction was taken into account through use of the DFT-D2 method.[36] The interaction strength between a single Au atom and a S atom of the PTM was found to be 0.16 eV. Reported results are those from calculations without Au atoms.

■ ASSOCIATED CONTENT

Supporting Information

Further details about chemical synthesis, EMBJ and MCBJ measurements, and DFT calculations. Additional measurements with gate and on the αH nonradical molecule are provided. This material is available free of charge via the Internet at http://pubs.acs.org.

■ AUTHOR INFORMATION

Corresponding Author

*E-mail: e.burzurilinares@tudelft.nl.

Author Contributions

R.F. and R.G. contributed the same.

Notes

The authors declare no competing financial interest.

■ ACKNOWLEDGMENTS

This work was supported by the EU FP7 program through project 618082 ACMOL and ERC grants advanced (Mols@Mols) and StG 2012-306826 e-GAMES. It was also supported by the Dutch Organization for Fundamental research (FOM), OCW, NWO(VENI), the Networking Research Center on Bioengineering, Biomaterials and Nanomedicine (CIBER-BBN) DGI (Spain) with projects BE-WELL CTQ2013-40480-R and MAT2012-30924, and Generalitat de Catalunya (2014-SGR-17, 2014-SGR-97, XRQTC, and a FI-DGR PhD grant for I.A. C.F. acknowledges CSIC for his Ph.D. bursary and he is enrolled in the Materials Science Ph.D. program of UAB. We also acknowledge use of supercomputing resources provided by the Red Española de Supercomputacion.

■ REFERENCES

(1) Gomberg, M. *J. Am. Chem. Soc.* **1900**, *22*, 757−771.
(2) Hicks, R. G. *Stable Radicals: Fundamentals and Applied Aspects of Odd-Electron Compounds*; John Wiley and Sons, Ltd: New York, 2010.
(3) Ratera, I.; Veciana, J. *Chem. Soc. Rev.* **2012**, *41*, 303−349.
(4) Rocha, A. R.; Garcia-Suarez, V. M.; Bailey, S. W.; Lambert, C. J.; Ferrer, J.; Sanvito, S. *Nat. Mater.* **2005**, *4*, 335−339.
(5) Mas-Torrent, M.; Crivillers, N.; Rovira, C.; Veciana, J. *Chem. Rev.* **2012**, *112*, 2506−2527.
(6) Crivillers, N.; Munuera, C.; Mas-Torrent, M.; Simao, C.; Bromley, S. T.; Ocal, C.; Rovira, C.; Veciana, J. *Adv. Mater.* **2009**, *21*, 1177−1181.
(7) Crivillers, N.; Paradinas, M.; Mas-Torrent, M.; Bromley, S. T.; Rovira, C.; Ocal, C.; Veciana, J. *Chem. Commun.* **2011**, *47*, 4664−4666.
(8) Simao, C.; Mas-Torrent, M.; Crivillers, N.; Lloveras, V.; Artes, J. M.; Gorostiza, P.; Veciana, J.; Rovira, C. *Nat. Chem.* **2011**, *3*, 359−364.
(9) Liu, J.; Isshiki, H.; Katoh, K.; Morita, T.; Breedlove, B. K.; Yamashita, M.; Komeda, T. *J. Am. Chem. Soc.* **2013**, *135*, 651−658.
(10) Zhang, Y. H.; Kahle, S.; Herden, T.; Stroh, C.; Mayor, M.; Schlickum, U.; Ternes, M.; Wahl, P.; Kern, K. *Nat. Commun.* **2013**, *4*, 2110.
(11) Mullegger, S.; Rashidi, M.; Fattinger, M.; Koch, R. *J. Phys. Chem. C* **2013**, *117*, 5718−5721.
(12) Parks, J. J.; Champagne, A. R.; Costi, T. A.; Shum, W. W.; Pasupathy, A. N.; Neuscamman, E.; Flores-Torres, S.; Cornaglia, P. S.; Aligia, A. A.; Balseiro, C. A.; Chan, G. K. L.; Abruna, H. D.; Ralph, D. C. *Science* **2010**, *328*, 1370−1373.
(13) Kondo, J. *Prog. Theor. Phys.* **1964**, *32*, 37−49.
(14) Goldhaber-Gordon, D.; Shtrikman, H.; Mahalu, D.; Abusch-Magder, D.; Meirav, U.; Kastner, M. A. *Nature* **1998**, *391*, 156−159.
(15) Parks, J. J.; Champagne, A. R.; Hutchison, G. R.; Flores-Torres, S.; Abruna, H. D.; Ralph, D. C. *Phys. Rev. Lett.* **2007**, *99*, 026601.
(16) Yu, L. H.; Natelson, D. *Nano Lett.* **2004**, *4*, 79−83.

DOI: 10.1021/acs.nanolett.5b00155
Nano Lett. XXXX, XXX, XXX−XXX

(17) Osorio, E. A.; O'Neill, K.; Wegewijs, M.; Stuhr-Hansen, N.; Paaske, J.; Bjornholm, T.; van der Zant, H. S. J. *Nano Lett.* **2007**, *7*, 3336−3342.
(18) Scott, G. D.; Natelson, D. *ACS Nano* **2010**, *4*, 3560−3579.
(19) Scott, G. D.; Natelson, D.; Kirchner, S.; Munoz, E. *Phys. Rev. B* **2013**, *87*, 241104(R).
(20) Liang, W.; Shores, M. P.; Bockrath, M.; Long, J. R.; Park, H. *Nature* **2002**, *417*, 725−729.
(21) Wagner, S.; Kisslinger, F.; Ballmann, S.; Schramm, F.; Chandrasekar, R.; Bodenstein, T.; Fuhr, O.; Secker, D.; Fink, K.; Ruben, M.; Weber, H. B. *Nat. Nanotechnol.* **2013**, *8*, 575−579.
(22) Armet, O.; Veciana, J.; Rovira, C.; Riera, J.; Castaner, J.; Molins, E.; Rius, J.; Miravitlles, C.; Olivella, S.; Brichfeus, J. *J. Phys. Chem.* **1987**, *91*, 5608−5616.
(23) Hakkinen, H. *Nat. Chem.* **2012**, *4*, 443−455.
(24) Ratner, M. *Nat. Nanotechnol.* **2013**, *8*, 378−381.
(25) Park, H.; Lim, A. K. L.; Alivisatos, A. P.; Park, J.; McEuen, P. L. *Appl. Phys. Lett.* **1999**, *75*, 301−303.
(26) O'Neill, K.; Osorio, E. A.; van der Zant, H. S. J. *Appl. Phys. Lett.* **2007**, *90*, 133109.
(27) de la Vega, L.; Martin-Rodero, A.; Agrait, N.; Yeyati, A. L. *Phys. Rev. B* **2006**, *73*, 075428.
(28) Thijssen, W. H. A.; Djukic, D.; Otte, A. F.; Bremmer, R. H.; van Ruitenbeek, J. M. *Phys. Rev. Lett.* **2006**, *97*, 226806.
(29) Goldhaber-Gordon, D.; Gores, J.; Kastner, M. A.; Shtrikman, H.; Mahalu, D.; Meirav, U. *Phys. Rev. Lett.* **1998**, *81*, 5225−5228.
(30) Nagaoka, K.; Jamneala, T.; Grobis, M.; Crommie, M. F. *Phys. Rev. Lett.* **2002**, *88*, 077205.
(31) Costi, T. A. *Phys. Rev. Lett.* **2000**, *85*, 1504−1507.
(32) Stephens, P. J.; Devlin, F. J.; Chabalowski, C. F.; Frisch, M. J. *J. Phys. Chem.* **1994**, *98*, 11623−11627.
(33) Frisch, M. J.; Trucks, G. W.; Schlegel, H. B.; Scuseria, G. E.; Robb, M. A.; Cheeseman, J. R.; Scalmani, G.; Barone, V.; Mennucci, B.; Petersson, G. A.; Nakatsuji, H.; Caricato, M.; Li, X.; Hratchian, H. P.; Izmaylov, A. F.; Bloino, J.; Zheng, G.; Sonnenberg, J. L.; Hada, M.; Ehara, M.; Toyota, K.; Fukuda, R.; Hasegawa, J.; Ishida, M.; Nakajima, T.; Honda, Y.; Kitao, O.; Nakai, H.; Vreven, T.; Montgomery, J. A., Jr.; Peralta, P. E.; Ogliaro, F.; Bearpark, M.; Heyd, J. J.; Brothers, E.; Kudin, K. N.; Staroverov, V. N.; Kobayashi, R.; Normand, J.; Raghavachari, K.; Rendell, A.; Burant, J. C.; Iyengar, S. S.; Tomasi, J.; Cossi, M.; Rega, N.; Millam, N. J.; Klene, M.; Knox, J. E.; Cross, J. B.; Bakken, V.; Adamo, C.; Jaramillo, J.; Gomperts, R.; Stratmann, R. E.; Yazyev, O.; Austin, A. J.; Cammi, R.; Pomelli, C.; Ochterski, J. W.; Martin, R. L.; Morokuma, K.; Zakrzewski, V. G.; Voth, G. A.; Salvador, P.; Dannenberg, J. J.; Dapprich, S.; Daniels, A. D.; Farkas, Ö.; Ortiz, J. V.; Cioslowski, J.; Fox, D. J. *Gaussian 09*, revision A.08; Gaussian, Inc.: Wallingford, CT, 2009.
(34) van Ruitenbeek, J. M.; Alvarez, A.; Pineyro, I.; Grahmann, C.; Joyez, P.; Devoret, M. H.; Esteve, D.; Urbina, C. *Rev. Sci. Instrum.* **1996**, *67*, 108−111.
(35) Martin, C. A.; Smit, R. H. M.; Egmond, R. v.; van der Zant, H. S. J.; van Ruitenbeek, J. M. *Rev. Sci. Instrum.* **2011**, *82*, 053907.
(36) Grimme, S. *J. Comput. Chem.* **2006**, *27*, 1787−1799.

DOI: 10.1021/acs.nanolett.5b00155
Nano Lett. XXXX, XXX, XXX−XXX